Scientific Research and Essays Vol. 7(43), pp. 3737-3750, 5 November, 2012
Available online at http://www.academicjournals.org/SRE
DOI: 10.5897/SRE12.316
ISSN 1992-2248 ©2012 Academic Journals

Full Length Research Paper

Influence of heat and mass transfer on Phan-Thien-Tanner fluid model for blood flow through a tapered artery with a stenosis

Noreen Sher Akbar[1]*, S. Nadeem[2] and Changhoon Lee[3]

[1]DBS&H, CEME, National University of Sciences and Technology, Islamabad, Pakistan.
[2]Department of Mathematics, Quaid-i-Azam University, 45320 Islamabad, 44000 Pakistan.
[3]Department of Computational Science and Engineering, Yonsei University, Seoul, Korea.

Accepted 16 July, 2012

In the present investigation, we study the influence of heat and mass transfer on blood flow through tapered artery with a stenosis. The non-Newtonian nature of blood in small arteries is analyzed mathematically by considering the blood as Phan-Thien-Tanner fluid. The representation for the blood flow is through an axially symmetrical stenosis. Symmetry of the distribution of the wall shearing stress and resistive impedance and their growth with the developing stenosis is another important feature of our analysis. Exact solutions are evaluated for velocity, temperature, concentration, resistance impedance, wall shear stress and shearing stress at the stenosis throat. The graphical results of different type of tapered arteries (that is, converging tapering, diverging tapering, non tapered artery) are examined for different parameters of interest.

Key words: Phan-Thien-Tanner fluid, blood flow, tapered artery, stenosis, exact solutions, heat and mass transfer.

INTRODUCTION

Recently, study of the effects of heat and mass transfer on blood has become quite interesting to many researchers both from the theoretical and experimental point of view because the quantitative prediction of blood flow rate and heat generation are of great importance for diagnosing blood circulation illness and for the noninvasive measurement of blood glucose (Chakravarty and Sen, 2005). Ma et al. (1994) studied heat and mass transfer in a separated flow region for high Prandtl and Schmidt numbers under pulsatile conditions. They analyzed in detail the arterial system and the hemodynamic factors that affect significantly blood phase transport and the vessel wall characteristics. Kawase and Ulbrecht (1983) examined the heat and mass transfer in non-Newtonian fluids. According to them the effect of non-Newtonian property of blood is small in the larger arteries where the shear rate is high. A vast amount of literature is available to study the non-Newtonian property of different fluid flows (Nadeem et al., 2009a, b; Abd El Hakeem, 2009; Phan-Thien and Tanner, 1977; Phan-Thien, 1978; Mekheimer and El Kot, 2008; Ellahi, 2010; Afsar Khan et al., 2012; Ellahi et al., 2010; Asghar et al., 2008; Ellahi, 2009). Valencia and Villanueva (2006) reported the unsteady flow and mass transfer in models of stenotic arteries considering fluid-structure interaction. The effect of heat transfer on the motion of blood in a diseased artery has been modeled by Ogulu and Abbey (2005). The influence of pulsatile laminar flow and heating protocol on temperature distribution in a single blood vessel and tumor tissue receiving hyperthermia treatment was taken into account by Khanafer et al. (2007). Motivated from the above analysis, we have studied the effects of heat and mass transfer on Phan-Thien-Tanner fluid model for blood flow through a tapered artery with a stenosis. To the best of author's knowledge no investigation has been made to study the blood flow

*Corresponding author. E-mail: noreensher@yahoo.com.

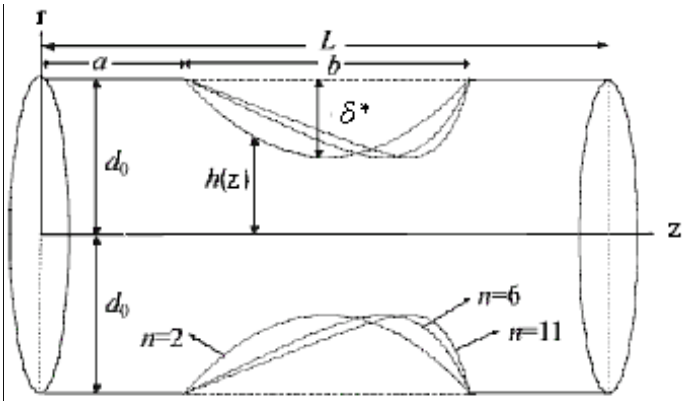

Figure 1. Geometry of an axially symmetrical stenosis in the artery.

by treating blood as Phan-Thien-Tanner fluid. The Phan-Thien-Tanner fluid is a non-Newtonian viscoelastic fluid model having shear thinning and shear thickening properties making it quite a useful model for blood flow analysis. Hence we are presenting a new original contribution for blood flow literature. Exact solutions of the simplified governing equations along with the boundary conditions of stenosed symmetric artery have been calculated. The expressions for velocity, temperature, concentration, resistance impedance, wall shear stress and shearing stress at the stenosis throat have been examined. The graphical behavior of different type of tapered arteries has been examined for different parameters of interest. Streamlines have been plotted at the end of the article.

PROBLEM FORMULATION

Let us consider an incompressible Phan-Thien-Tanner fluid having constant viscosity μ and density ρ in a tube having length L. We are considering a cylindrical coordinate system (r, θ, z) such that $\bar{u}$ and $\bar{w}$ are the velocity component in $\bar{r}$ and $\bar{z}$ direction respectively. Further we assume that $r = 0$ is taken as the axis of the symmetry of the tube. Heat and mass transfer phenomena is taken into account by giving temperature $\bar{T}_1$ and concentration $\bar{C}_1$ to the wall of the tube, while at the centre of the tube we are considering axial symmetry condition on both temperature and concentration. The geometry of the stenosis which is assumed to be axially symmetric can be described as in Ellahi (2010).

$$h(z) = d(z)\left[1-\eta\left(b^{n-1}(z-a)-(z-a)^n\right)\right], \quad a \le z \le a+b, \quad = d(z), \text{ otherwise} \tag{1}$$

with

$$d(z) = d_0 + \xi z,\ \eta = \frac{\delta^* n^{\frac{n}{n-1}}}{d_0 b^n (n-1)}, \tag{2}$$

where $d(z)$ is the radius of the tapered arterial segment in the stenotic region, d_0 is the radius of the non-tapered artery in the non-stenoic region, ξ is the tapering parameter, b is the length of stenosis, $n \ge 2$ is a parameter determining the shape of the constriction profile and referred to as the shape parameter, a and b indicates its location as shown in Figure 1. The parameter η is defined as in Figure 1 in which δ^* denotes the maximum height of the stenosis located at

$$z = a + \frac{b}{n^{\frac{n}{4-n}}}. \tag{3}$$

The equations governing the steady incompressible fluid are defined as

$$\frac{\partial \bar{u}}{\partial \bar{r}} + \frac{\bar{u}}{\bar{r}} + \frac{\partial \bar{w}}{\partial \bar{z}} = 0,$$

$$\rho\left(\bar{u}\frac{\partial}{\partial \bar{r}} + \bar{w}\frac{\partial}{\partial \bar{z}}\right)\bar{u} = -\frac{\partial \bar{p}}{\partial \bar{r}} + \frac{1}{\bar{r}}\frac{\partial}{\partial \bar{r}}\left(\bar{r}\,\bar{\tau}_{\bar{r}\bar{r}}\right) + \frac{\partial}{\partial \bar{z}}\left(\bar{\tau}_{\bar{r}\bar{z}}\right) - \frac{\bar{\tau}_{\bar{\theta}_1\bar{\theta}_1}}{\bar{r}}, \tag{4}$$

$$\rho\left(\bar{u}\frac{\partial}{\partial \bar{r}} + \bar{w}\frac{\partial}{\partial \bar{z}}\right)\bar{w} = -\frac{\partial \bar{p}}{\partial \bar{z}} + \frac{1}{\bar{r}}\frac{\partial}{\partial \bar{r}}\left(\bar{r}\,\bar{\tau}_{\bar{r}\bar{z}}\right) + \frac{\partial}{\partial \bar{z}}\left(\bar{\tau}_{\bar{z}\bar{z}}\right), \tag{5}$$

$$\rho c_p\left(\bar{u}\frac{\partial}{\partial \bar{r}} + \bar{w}\frac{\partial}{\partial \bar{z}}\right)\bar{T} = \bar{\tau}_{\bar{r}\bar{r}}\frac{\partial \bar{u}}{\partial \bar{r}} + \bar{\tau}_{\bar{r}\bar{z}}\frac{\partial \bar{w}}{\partial \bar{r}} + \bar{\tau}_{\bar{z}\bar{r}}\frac{\partial \bar{u}}{\partial \bar{z}} + \bar{\tau}_{\bar{z}\bar{z}}\frac{\partial \bar{w}}{\partial \bar{z}} + k\left(\frac{\partial^2 \bar{T}}{\partial \bar{r}^2} + \frac{1}{\bar{r}}\frac{\partial \bar{T}}{\partial \bar{r}} + \frac{\partial^2 \bar{T}}{\partial \bar{z}^2}\right), \tag{6}$$

$$\left(\bar{u}\frac{\partial}{\partial \bar{r}} + \bar{w}\frac{\partial}{\partial \bar{z}}\right)\bar{C} = D\left(\frac{\partial^2 \bar{C}}{\partial \bar{r}^2} + \frac{1}{\bar{r}}\frac{\partial \bar{C}}{\partial \bar{r}} + \frac{\partial^2 \bar{C}}{\partial \bar{z}^2}\right) + \frac{DK_T}{T_m}\left(\frac{\partial^2 \bar{T}}{\partial \bar{r}^2} + \frac{1}{\bar{r}}\frac{\partial \bar{T}}{\partial \bar{r}} + \frac{\partial^2 \bar{T}}{\partial \bar{z}^2}\right). \tag{7}$$

In the above equations, $\bar{p}$ is the pressure; $\bar{u}$, $\bar{w}$ are the respective velocity components in the radial and axial directions respectively; $\bar{T}$ is the temperature; $\bar{C}$ is the concentration of fluid; k denotes the thermal conductivity; c_p is the specific heat at constant pressure; T_m is the temperature of the medium; D is the

coefficient of mass diffusivity, K_T is the thermal-diffusion ratio.

The constitutive equation for Phan-Thien-Tanner fluid is defined by Abd El Hakeem (2009), Phan-Thien and Tanner (1977) and Phan-Thien (1978) as

$$f\left(tr\left(\bar{\boldsymbol{\tau}}\right)\right)\bar{\boldsymbol{\tau}}+k_1\bar{\boldsymbol{\tau}}^{\nabla}=2\mu\mathbf{D} \tag{8}$$

Where

$$\bar{\boldsymbol{\tau}}^{\nabla}=\frac{\partial\bar{\boldsymbol{\tau}}}{\partial t}+\left(v.\nabla\right)\bar{\boldsymbol{\tau}}-\bar{\boldsymbol{\tau}}.\nabla v-\left(\nabla v\right)^{T}.\bar{\boldsymbol{\tau}} \tag{8a}$$

$$f\left(tr\left(\bar{\boldsymbol{\tau}}\right)\right)=1+\frac{\varepsilon k_1}{\mu}tr\left(\bar{\boldsymbol{\tau}}\right), \tag{8b}$$

$$f\left(tr\left(\bar{\boldsymbol{\tau}}\right)\right)=\exp\left(\frac{\varepsilon k_1}{\mu}tr\left(\bar{\boldsymbol{\tau}}\right)\right), \tag{8c}$$

in which $\bar{\boldsymbol{\tau}}$ is shear stress tensor, T denotes the transpose, v is velocity, ε is extensional parameter, D is the deformation rate tensor, k_1 is the relaxation time, μ is the constant viscosity coefficient and $\bar{\boldsymbol{\tau}}^{\nabla}$ denotes Oldroyd's upper-convected derivative.

We introduce the non-dimensional variables

$$\begin{gathered}
r=\frac{\bar{r}}{d_0},\ z=\frac{\bar{z}}{b},\ w=\frac{\bar{w}}{u_0},\ u=\frac{b\bar{u}}{u_0\delta},\ p=\frac{d_0^2\bar{p}}{u_0b\mu},\ h=\frac{\bar{h}}{d_0},\\
\mathrm{Re}=\frac{\rho bu_0}{\mu},\ \tilde{\boldsymbol{\tau}}_{rr}=\frac{b\bar{\boldsymbol{\tau}}_{rr}}{u_0\mu},\ \tilde{\boldsymbol{\tau}}_{rz}=\frac{d_0\bar{\boldsymbol{\tau}}_{rz}}{u_0\mu},\ \tilde{\boldsymbol{\tau}}_{zz}=\frac{b\bar{\boldsymbol{\tau}}_{zz}}{u_0\mu},\ We=\frac{k_1u_0}{d_0},\\
S_r=\frac{\rho DK_T\bar{T}_0}{\mu T_m\bar{C}_0},\ S_c=\frac{\mu}{D\rho},\ \sigma=\frac{\left(\bar{C}-\bar{C}_0\right)}{\bar{C}_0},\\
\theta=\frac{\bar{T}-\bar{T}_0}{\bar{T}_0},\ E_c=\frac{u_0^2}{c_p\bar{T}_0},\ \mathrm{Pr}=\frac{c_p\mu}{k}.
\end{gathered} \tag{9}$$

Here u_0 is the velocity averaged over the section of the tube of the width d_0.

Here Equation (9) was used; Equations (3) to (8) - the appropriate equations describing the steady flow of an incompressible Phan-Thien-Tanner fluid in the case of mild stenosis $\left(\frac{\delta^*}{d_0}<<1\right)$ subject to the additional conditions (Mekheimer and El Kot, 2008)

$$(i)\ \frac{\mathrm{Re}\,\delta^*n^{\left(\frac{1}{n-1}\right)}}{b}<<1, \tag{10a}$$

$$(ii)\ \frac{d_0n^{\left(\frac{1}{n-1}\right)}}{b}\sim O(1), \tag{10b}$$

Using the dimensionless quantities, the governing continuity, momentum, energy and concentration equation in dimensionless form are as in Equations (11) to (15)

$$\frac{\partial u}{\partial r}+\frac{u}{r}+\frac{\partial w}{\partial z}=0, \tag{11}$$

$$\frac{\partial p}{\partial r}=0, \tag{12}$$

$$\frac{\partial p}{\partial z}=\frac{1}{r}\frac{\partial\left(r\tilde{\tau}_{rz}\right)}{\partial r}, \tag{13}$$

$$\frac{1}{r}\frac{\partial}{\partial r}\left(r\frac{\partial\theta}{\partial r}\right)+B_r\left(\frac{\partial w}{\partial r}\right)\tilde{\tau}_{rz}=0, \tag{14}$$

$$\frac{1}{S_c}\frac{1}{r}\frac{\partial}{\partial r}\left(r\frac{\partial\sigma}{\partial r}\right)+\frac{S_r}{r}\frac{\partial}{\partial r}\left(r\frac{\partial\theta}{\partial r}\right)=0, \tag{15}$$

where $B_r=E_cP_r$ is Brinkmann number.

$$f\tilde{\boldsymbol{\tau}}_{zz}=2We\tilde{\boldsymbol{\tau}}_{rz}\frac{\partial w}{\partial r}, \tag{16a}$$

$$f\tilde{\boldsymbol{\tau}}_{rz}=\frac{\partial w}{\partial r}+We\tilde{\boldsymbol{\tau}}_{rr}\frac{\partial u}{\partial r}, \tag{16b}$$

$$f=1+\varepsilon We\left(\tilde{\boldsymbol{\tau}}_{rr}+\tilde{\boldsymbol{\tau}}_{\theta\theta}+\tilde{\boldsymbol{\tau}}_{zz}\right). \tag{16c}$$

$$f=\exp\left(\varepsilon We\left(\tilde{\boldsymbol{\tau}}_{rr}+\tilde{\boldsymbol{\tau}}_{\theta\theta}+\tilde{\boldsymbol{\tau}}_{zz}\right)\right). \tag{16d}$$

For the case of small stenosis $\left(\frac{\delta^*}{d_0}<<1\right)$ and using conditions (10a) and (10b) we get $\tilde{\boldsymbol{\tau}}_{\theta_1\theta_1}=0$ and $\tilde{\boldsymbol{\tau}}_{rr}=0$ and thus trace of stress tensor becomes $\tilde{\boldsymbol{\tau}}_{zz}$. In this situation, it is easy to verify from the equations of motion that pressure gradient $\frac{dp}{dz}$ is only a function of z and the integration of the longitudinal momentum equation subjected to the boundary conditions $\tilde{\boldsymbol{\tau}}_{rz}=0$ at the symmetry line $r=0,$ yields

$$\tilde{\boldsymbol{\tau}}_{rz}=\frac{r}{2}\frac{dp}{dz}, \tag{17}$$

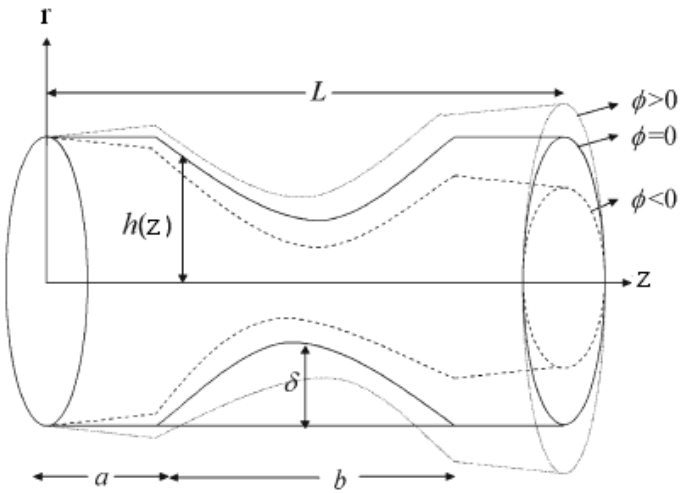

Figure 2. Geometry of the axially stenosied tapered artery for different tapered angle.

with the above simplifications and upon the division of the expressions for the two non vanishing stresses, Equations (16a) and (16b) the function f is cancelled out resulting in

$$\tilde{\tau}_{zz} = 2We\tilde{\tau}_{rz}^2, \tag{18}$$

Linear PTT Model

Using Equations (16c) when $\tilde{\tau}_{rr} = 0$ and $\tilde{\tau}_{\theta\theta} = 0$ and substituting Equation (18) into (16b), we obtain

$$\frac{\partial w}{\partial r} = \tilde{\tau}_{rz} + 2\varepsilon We^2\tilde{\tau}_{rz}^3 \tag{19a}$$

Exponential PTT Model

Using Equation (16d) when $\tilde{\tau}_{rr} = 0$ and $\tilde{\tau}_{\theta\theta} = 0$ and substituting Equation (18) into (16b), we obtain

$$\frac{\partial w}{\partial r} = \tilde{\tau}_{rz}\exp\left(2\varepsilon We^2\tilde{\tau}_{rz}^2\right) \tag{19b}$$

The final expressions for energy and mass concentration equations take the form

$$\frac{1}{r}\frac{\partial}{\partial r}\left(r\frac{\partial\theta}{\partial r}\right) + B_r\left(\left(\frac{\partial w}{\partial r}\right)\frac{r}{2}\frac{dp}{dz}\right) = 0, \tag{20}$$

$$\frac{1}{S_c}\left(\frac{1}{r}\frac{\partial}{\partial r}\left(r\frac{\partial\sigma}{\partial r}\right)\right) + S_r\left(\frac{1}{r}\frac{\partial}{\partial r}\left(r\frac{\partial\theta}{\partial r}\right)\right) = 0. \tag{21}$$

The corresponding boundary conditions are

$$\frac{\partial w}{\partial r} = 0,\ \frac{\partial\theta}{\partial r} = 0,\ \frac{\partial\sigma}{\partial r} = 0 \text{ at } r = 0, \tag{22a}$$

$$w = 0,\ \theta = 0,\ \sigma = 0 \text{ at } r = h(z), \tag{22b}$$

Where

$$h(z) = (1+\xi z)\left[1-\eta\left((z-\sigma_1)-(z-\sigma_1)^n\right)\right],\quad \sigma_1 \le z \le \sigma_1 + 1, \tag{23}$$

and

$$\eta_1 = \frac{\delta n^{\frac{n}{n-1}}}{(n-1)},\ \delta = \frac{\delta^*}{d_0},\ \sigma_1 = \frac{a}{b},\ \xi' = \frac{\xi b}{d_0}, \tag{24}$$

in which $\xi = \tan\phi$ where ϕ is called tapered angle and for converging tapering $(\phi < 0)$, non-tapered artery $(\phi = 0)$ and the diverging tapering $(\phi > 0)$ as shown in Figure 2.

Solution of the problem

Exact solution

The exact solution of Equations (19) to (21) subjected to the boundary conditions (22a) and (22b) directly given as

$$w(r,z) = \left(\frac{r^2-h^2}{4}\right)\frac{dp}{dz} + \frac{\varepsilon We^2\left(r^4-h^4\right)}{16}\left(\frac{dp}{dz}\right)^3, \text{ For Linear PTT Model} \tag{25a}$$

$$w(r,z) = \frac{1}{2m_1 s}\left(\exp\left(sm_1^2r^2\right) - \exp\left(sm_1^2h^2\right)\right), \text{ For Exponential PTT Model} \tag{25b}$$

where $m_1 = \frac{dp}{dz},\ s = 2\varepsilon We^2.$

$$\theta(r,z) = -B_r\left(\left(\frac{r^4-h^4}{64}\right)\left(\frac{dp}{dz}\right)^2 + \frac{\varepsilon We^2\left(r^6-h^6\right)}{288}\left(\frac{dp}{dz}\right)^4\right), \tag{26}$$

$$\sigma(r,z)=S_r S_c B_r\left(\left(\frac{r^4-h^4}{64}\right)\left(\frac{dp}{dz}\right)^2+\frac{\varepsilon We^2\left(r^6-h^6\right)}{288}\left(\frac{dp}{dz}\right)^4\right). \quad (27)$$

We can define the volumetric flow rate Q by

$$Q=\int_0^h rwdr \quad (28)$$

Substituting Equation (25a) into (28) we get

$$\varepsilon We^2 h^6\left(\frac{dp}{dz}\right)^3+3h^4\frac{dp}{dz}+48Q=0. \quad 29)$$

From the Cardan-Tartaglia formula for the solution of algebraic cubic equation, the real solution of Equation (29) is

$$\frac{dp}{dz}=-\frac{1}{m}+\left(\frac{m}{\varepsilon We^2 h^2}\right). \quad \text{For linear PTT Model} \quad (30a)$$

where

$$m=\left(-d+\sqrt{\varepsilon^3 We^6 h^6+d^2}\right)^{\frac{1}{3}} \text{ and } d=12(2Q)\varepsilon^2 We^4.$$

Substituting Equation (25b) into (28) we get

$$\frac{dp}{dz}=\frac{1}{2m_1 s}\left(\frac{\sqrt{\pi}Erf\left[hm_1\sqrt{s}\right]}{2m_1\sqrt{s}}\right)-\frac{h}{2m_1 s}\exp\left(sm_1^2h^2\right)-F. \quad \text{For exponential PTT Model} \quad (30b)$$

The corresponding stream function can be found using the following formula

$$w=\frac{1}{r}\frac{\partial\Psi}{\partial r}.$$

The pressure drop $(\Delta p=p \text{ at } z=0 \text{ and } \Delta p=-p \text{ at } z=L)$ across the stenosis between the section $z=0$ and $z=L$ is obtained from (24) (Mekheimer and El Kot, 2008) as

$$\Delta p=\int_0^L\left(-\frac{dp}{dz}\right)dz. \quad (31)$$

Resistance impedance

The expression for resistance impedance is obtained from Equation (31) and is defined as follows

$$\tilde{\lambda}=\frac{\Delta p}{Q}=\left\{\int_0^a F(z)\big|_{h=1}dz+\int_a^{a+b}F(z)dz+\int_{a+b}^{L}F(z)\big|_{h=1}dz\right\} \quad (32)$$

Where

$$F(z)=-\frac{1}{m}+\left(\frac{m}{\varepsilon We^2 h^2}\right).$$

The simplified form of Equation (26) takes the following form

$$\tilde{\lambda}=\left\{(L-b)\left(-\frac{1}{m}+\left(\frac{m}{\varepsilon We^2}\right)\right)+\int_a^{a+b}F(z)dz\right\}. \quad (33)$$

Expression for the wall shear stress

The non zero dimensionless shear stress is shown as

$$\tilde{\boldsymbol{\tau}}_{rz}=\left(\frac{r}{2}\frac{dp}{dz}\right). \quad (34)$$

With the help of Equation (34) we can find the expression for wall shear stress at $r=h$ as

$$\tilde{\boldsymbol{\tau}}_{rz}=\left(\frac{h}{2}\frac{dp}{dz}\right). \quad (35)$$

We can note that the shearing stress at the stenosis throat, that is the wall shear at the maximum height of the stenosis located at $z=\frac{a}{b}+\frac{1}{n^{\frac{n}{4-n}}}$, that is $\tilde{\tau}_s=\tilde{\boldsymbol{\tau}}_{rz}\big|_{h=1-\delta}$

$$\tilde{\tau}_s=\left(\frac{(1-\delta)}{2}\frac{dp}{dz}\right). \quad (36)$$

The final expression for the dimensionless resistance to λ, wall shear stress $\boldsymbol{\tau}_{rz}$ and the shearing stress at the throat τ_s are defined as

$$\lambda=\frac{1}{3}\left\{\left(1-\frac{b}{L}\right)\left(-\frac{1}{m}+\left(\frac{m}{\varepsilon We^2}\right)\right)+\frac{1}{L}\int_a^{a+b}F(z)dz\right\}, \quad (37)$$

$$\boldsymbol{\tau}_{rz}=\left(\frac{h}{8Q}\frac{dp}{dz}\right), \quad (38)$$

$$\tau_s=\left(\frac{(1-\delta)}{8Q}\frac{dp}{dz}\right), \quad (39)$$

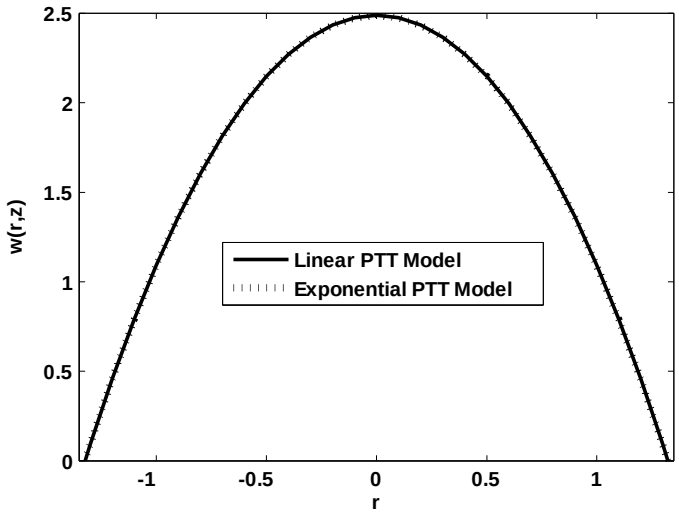

Figure 3. Variation of velocity profile for $Q = 0.3,\ n = 2,\ \sigma_1 = 0.0,\ \delta = 0.3,\ \varepsilon = 0.2,\ z = 0.5.$

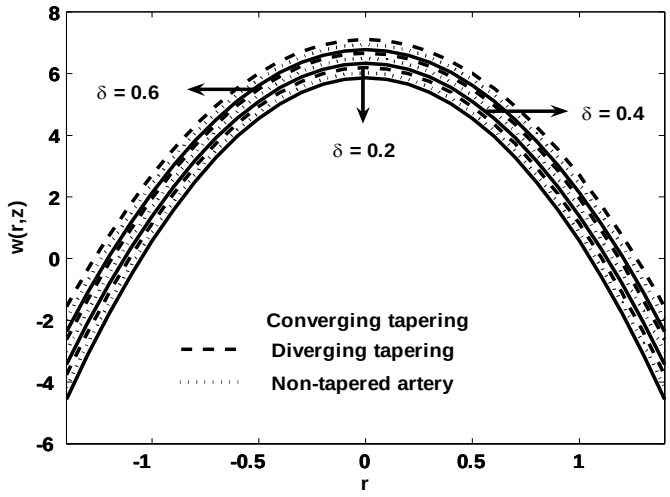

Figure 4. Variation of velocity profile for $Q = 0.3,\ We = 0.5,\ \sigma_1 = 0.0,\ \varepsilon = 0.1,\ n = 2,\ z = 0.5.$

in which

$$\lambda = \frac{\tilde{\lambda}}{\lambda_0},\ \boldsymbol{\tau}_{rz} = \frac{\tilde{\boldsymbol{\tau}}_{rz}}{\tau_0},\ \tau_s = \frac{\tilde{\tau}_s}{\tau_0},\ \lambda_0 = 3L,\ \tau_0 = 4Q,$$

λ_0 and τ_0 are the resistance to flow and the wall shear stress for a flow in a normal artery (no stenosis).

NUMERICAL RESULTS AND DISCUSSION

To observe the quantitative effects of the extensional parameter ε, Weissenberg number We, the stenosis shape n and maximum height of the stenosis δ for converging tapering, diverging tapering and non-tapered arteries for Phan-Thien-Tanner fluid Figures 3 to 14 are plotted. The variation of axial velocity for ε, We and δ for the case of a converging tapering, diverging tapering and non-tapered arteries are displayed in Figures 4 to 6 . In Figures 4 to 6 we observed that with an increase in We and ε, velocity profile increases while it decreases with an increase in δ. It is also seen that for the case of

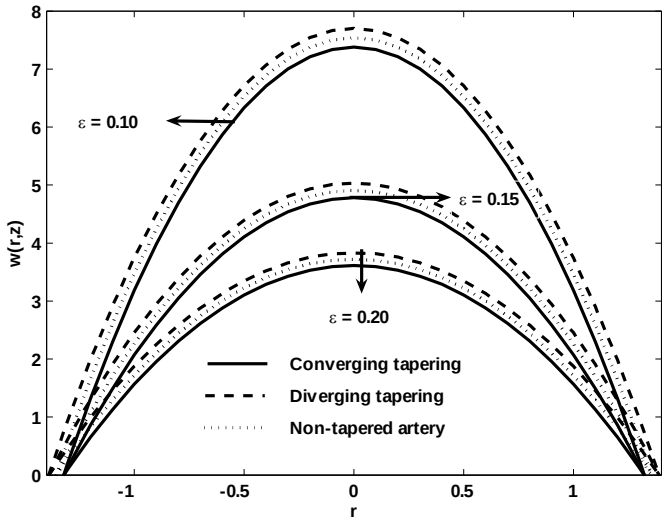

Figure 5. Variation of velocity profile for $Q = 0.3,\ We = 0.5,\ \sigma_1 = 0.0,\ \delta = 0.3,\ n = 2,\ z = 0.5.$

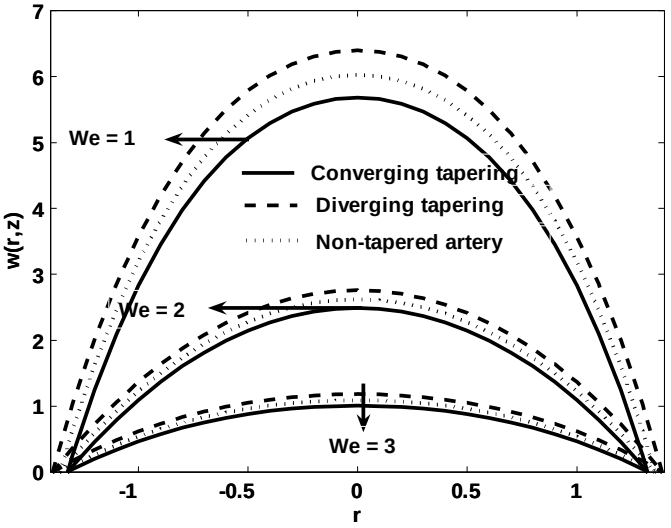

Figure 6. Variation of velocity profile for $Q = 0.3,\ n = 2,\ \sigma_1 = 0.0,\ \delta = 0.3,\ \varepsilon = 0.2,\ z = 0.5.$

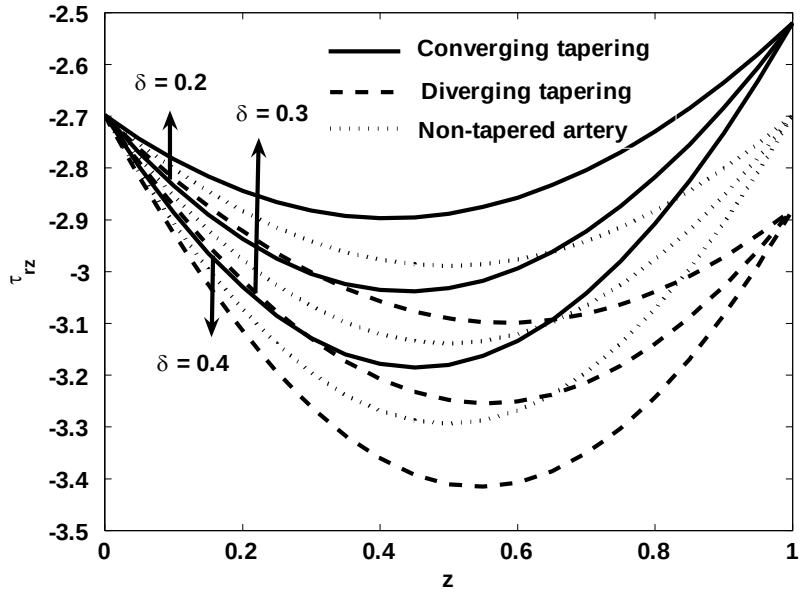

Figure 7. Variation of wall shear stress for $Q = 0.3,\ \varepsilon = 0.2,\ \sigma_1 = 0.0,$ $n = 2,\ We = 0.5.$

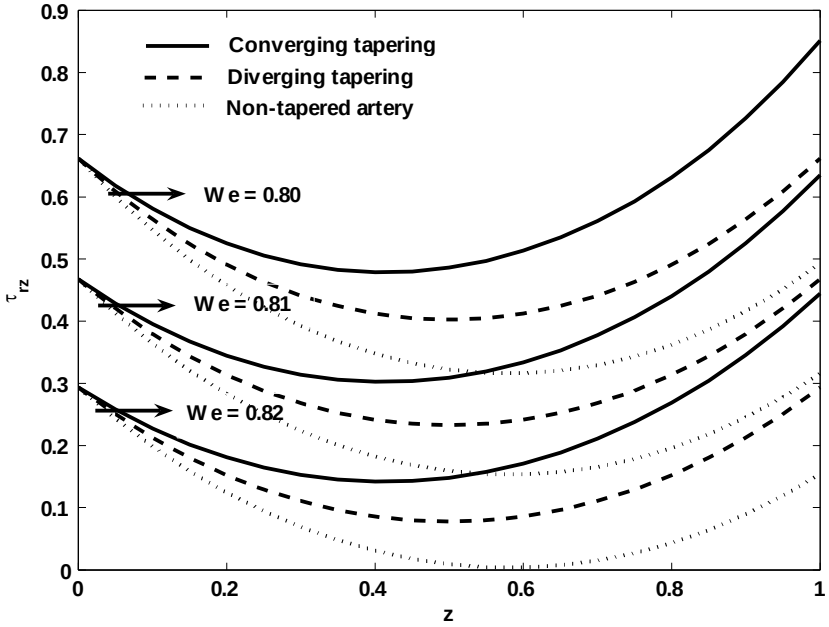

Figure 8. Variation of wall shear stress for $Q = 0.3,\ \varepsilon = 0.2,\ \sigma_1 = 0.0,$ $n = 2,\ \delta = 0.2.$

converging tapering velocity, it gives larger values as compared to the case of diverging tapering and non-tapered arteries. Figures 7 to 9 show how the converging tapering, diverging tapering and non-tapered arteries influence on the wall shear stress τ_{rz}. It is observed that with an increase in $We,\ \delta$ and n shear stress decreases, the stress yield diverging tapering with tapered angle $\phi > 0$, converging tapering with tapered angle $\phi < 0$ and non-tapered artery with tapered angle

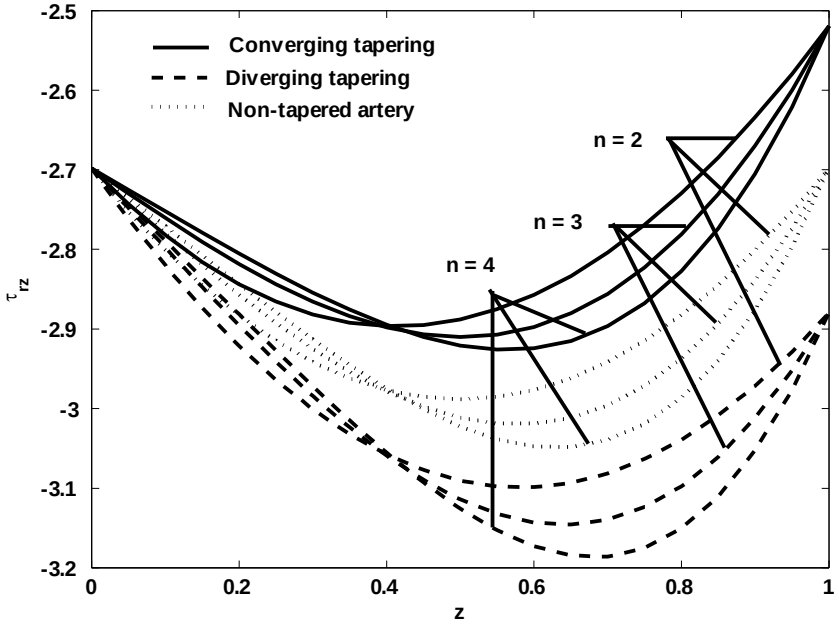

Figure 9. Variation of wall shear stress for $Q = 0.3,\ \varepsilon = 0.2,\ \sigma_1 = 0.0,$ $We = 0.5,\ \delta = 0.2.$

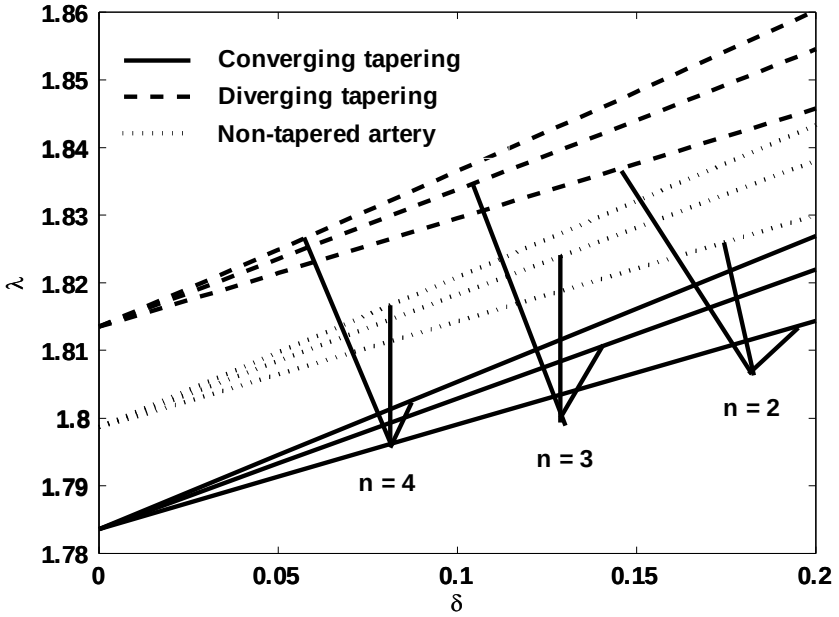

Figure 10. Variation of resistance for $Q = 0.3,\ b = 1,\ L = 1,\ \sigma_1 = 0.0,$ $\varepsilon = 0.5,\ We = 0.5.$

$\phi = 0$. In Figures 10 to 13 we noticed that the impedance resistance increases for converging tapering, diverging tapering and non-tapered arteries when we increase n and ε, while it decreases with the increase in We. We also observed that resistive impedance in a diverging tapering appear to be smaller than those in converging tapering because the flow rate is higher in the former than that in the latter, as anticipated and

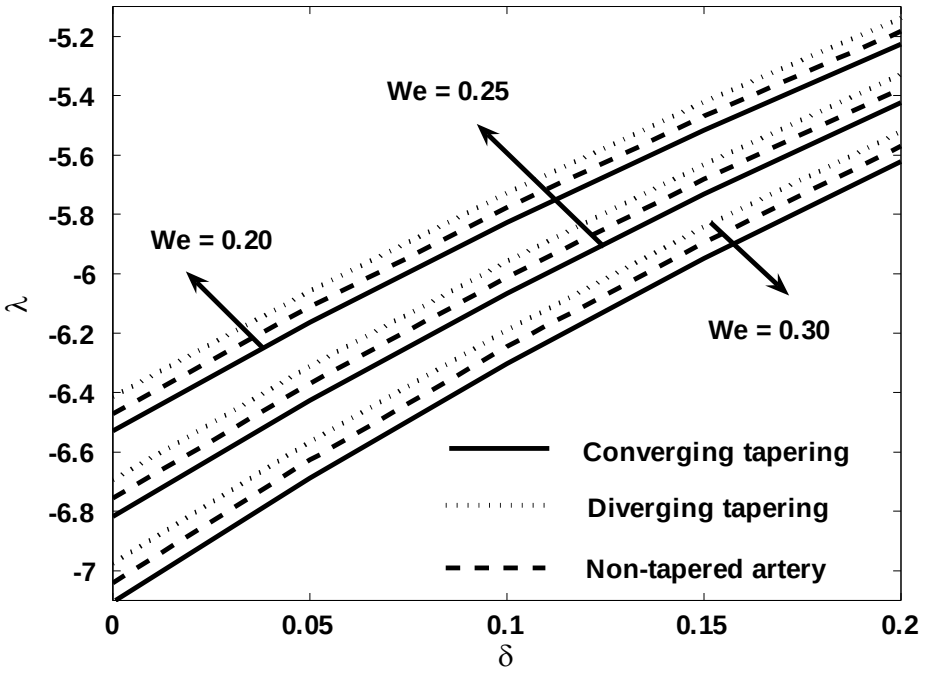

Figure 11. Variation of resistance for $Q=0.3,\ b=1,\ L=1,\ \sigma_1=0.0,\ \varepsilon=0.8,$ $n=11.$

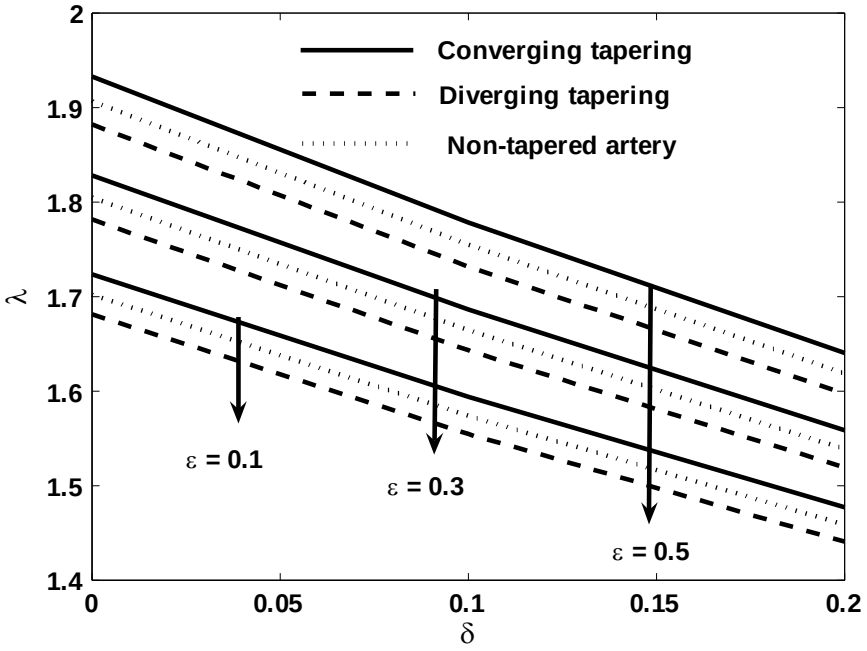

Figure 12. Variation of resistance for $Q=0.3,\ b=1,\ L=1,\ \sigma_1=0.0,$ $n=2,\ We=0.5.$

impedance resistance attains its maximum values in the symmetric stenosis case (n=2) . Finally Figures 14 and 15 are prepared to see the variation of the shearing stress at the stenosis throat τ_s with δ. It is analyzed

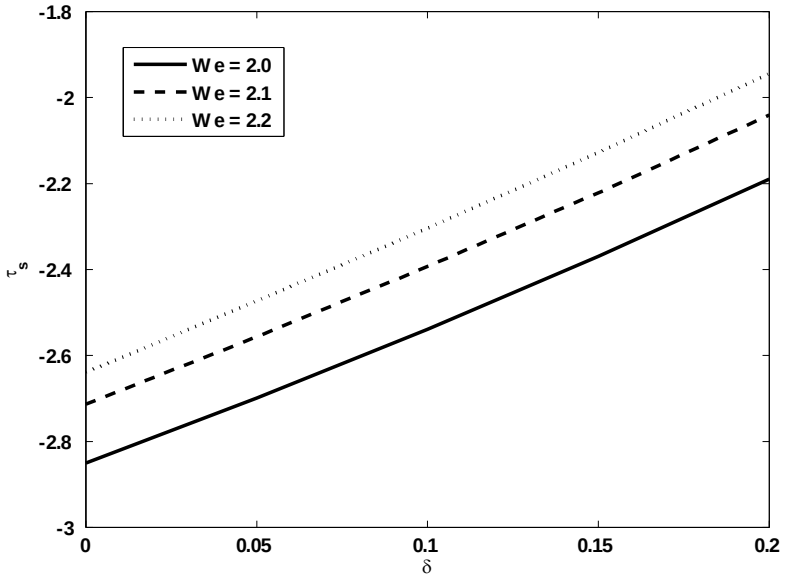

Figure 13. Variation of shear stress at the stenosis throat for $Q = 0.3$, $We = 0.5$.

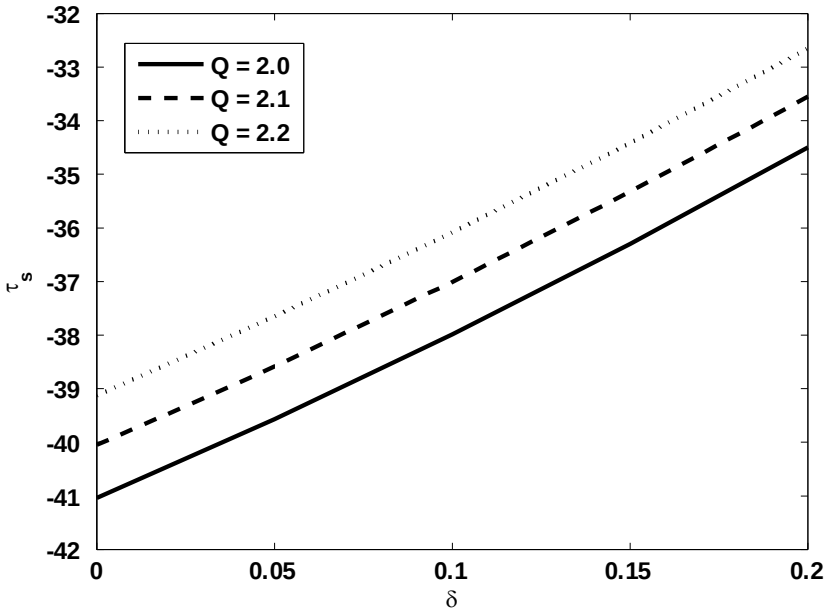

Figure 14. Variation of shear stress at the stenosis throat for $We = 0.5$, $\varepsilon = 0.2$.

through figures that shearing stress at the stenosis throat increases with an increase in ε, Q and We. Figures 16 and 17 show the variation of temperature profile for different values of Brickmann number B_r and Weissenberg number We. It is observed that with an increase in Brickmann number B_r, temperature profile increases; while it decreases with an increase in Weissenberg number We; also temperature profile gives the large values for converging tapering as compared to the diverging and non-tapered artery.

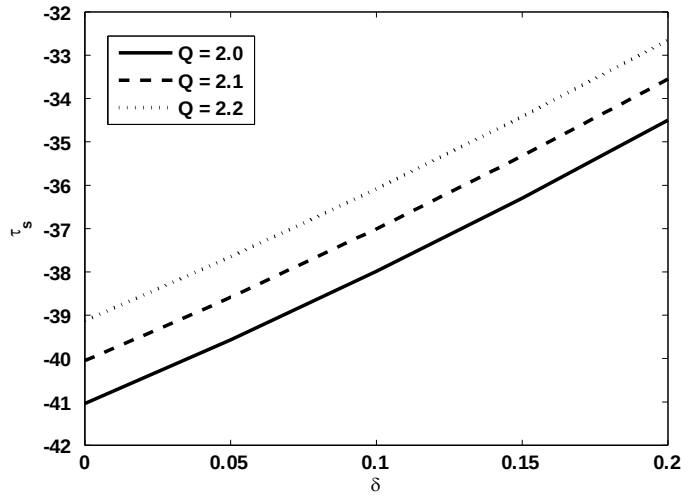

Figure 14. Variation of shear stress at the stenosis throat for $We = 0.5,\ \varepsilon = 0.2.$

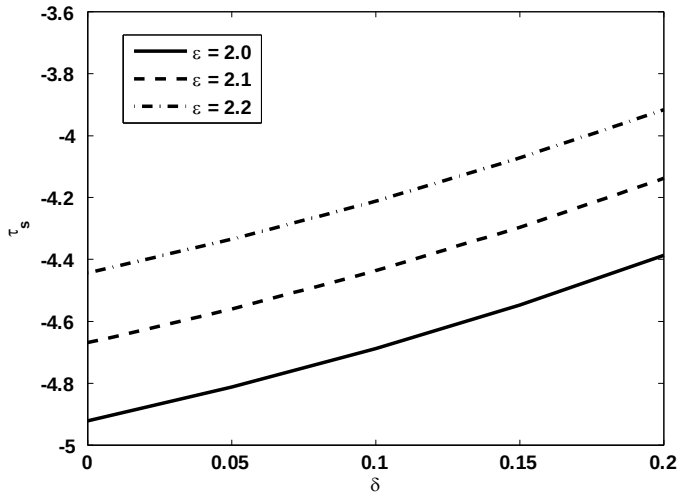

Figure 15. Variation of shear stress at the stenosis throat for $F = 0.5,\ \varepsilon = 0.2.$

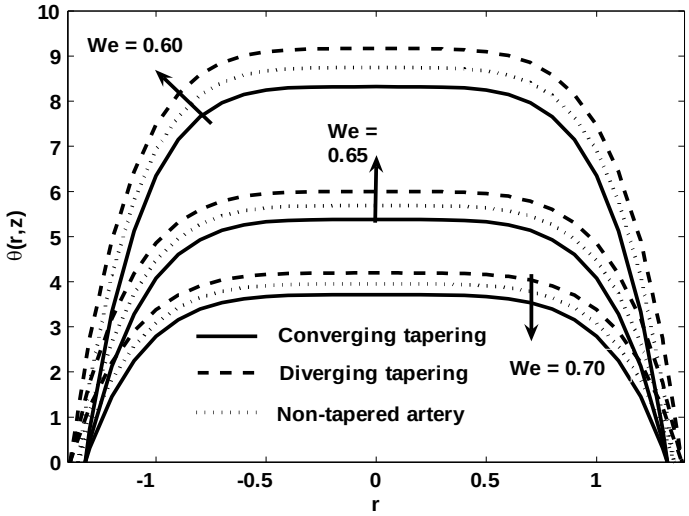

Figure 16. Variation of temperature profile for $Q = 0.3,\ n = 2,$ $\sigma_1 = 0.0,\ \delta = 0.3,\ \varepsilon = 0.2,\ z = 0.5,\ B_r = 0.5.$

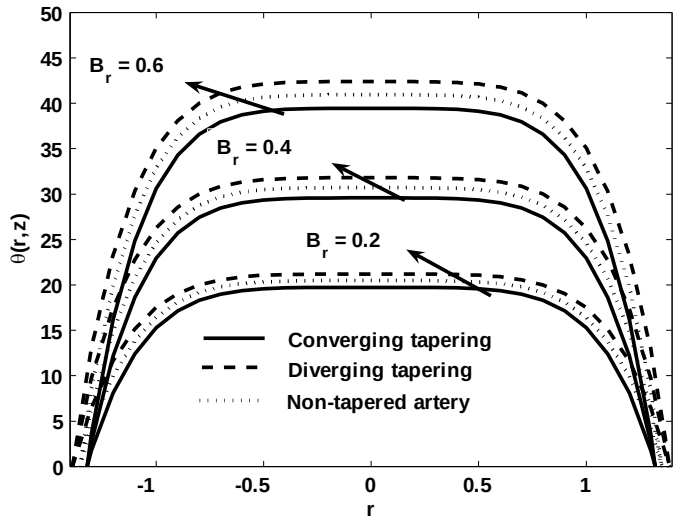

Figure 17. Variation of temperature profile for $Q = 0.3,\ n = 2,$ $\sigma_1 = 0.0,\ \delta = 0.3,\ \varepsilon = 0.2,\ z = 0.5,\ We = 0.5.$

Figures 18 to 20 are prepared to see the variation of concentration profile for Brickmann number B_r, Weissenberg number We and Soret number S_r. It is analyzed that with an increase in Brickmann number B_r and Soret number S_r concentration profile decreases, while it increases with an increase in Weissenberg number We. It is also observed that concentration profile has an opposite behavior as compared to the temperature profile. Trapping phenomena have been discussed through Figures 21 to 24. It is observed that with an increase in Weissenberg number We, the stenosis shape n and maximum height of the stenosis δ, number of trapping bolus increases and size of the trapping bolus decreases, while with an increase in extensional parameter ε, number of trapping bolus decreases and size of the trapping bolus increases.

Conclusion

The effects of Phan-Thien-Tanner fluid model for blood flow through a tapered artery with a stenosis are

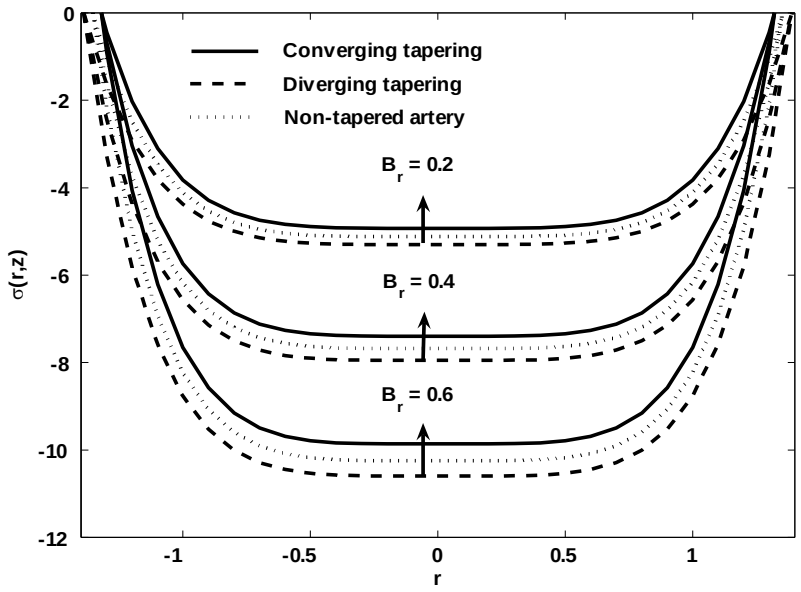

Figure 18. Variation of concentration profile for $Q = 0.3,\ n = 2,\ \sigma_1 = 0.0,$ $\delta = 0.3,\ \varepsilon = 0.2,\ z = 0.5,\ We = 0.5,\ S_r = 0.5,\ S_c = 0.5.$

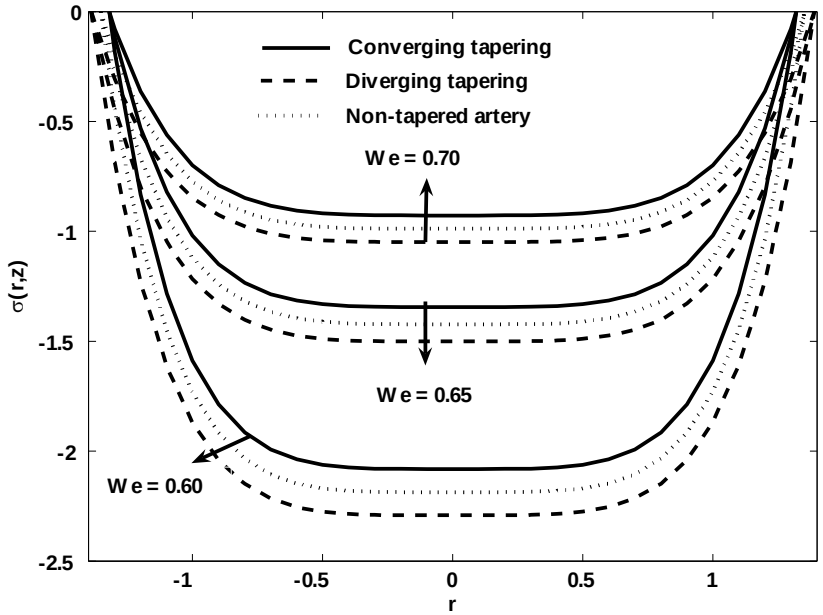

Figure 19. Variation of concentration profile for $Q = 0.3,\ n = 2,\ \sigma_1 = 0.0,$ $\delta = 0.3,\ \varepsilon = 0.2,\ z = 0.5,\ B_r = 0.5,\ S_r = 0.5,\ S_c = 0.5.$

investigated. The main points of presented analysis are listed below

1) It is observed that with an increase in We and ε velocity profile increases; while it decreases with an increase in δ.

2) It is noticed that for the case of converging tapering, velocity gives larger values as compared to the case of diverging tapering and non-tapered arteries. Because for converging tapering, flow easily passed from the arteries.

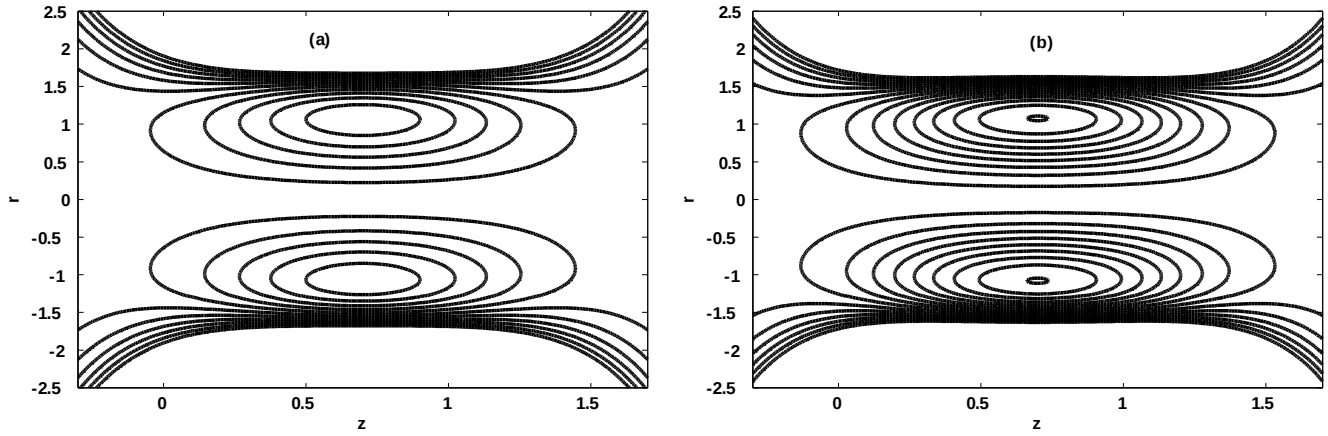

Figure 21. Stream lines for different values of δ (a) $\delta = 0.1$ (b) $\delta = 0.2$ other parameters are $\phi = \pi,\ \varepsilon = 0.1,\ Q = 0.1,\ \sigma = 0.4,$ $We = 0.3,\ n = 2.$

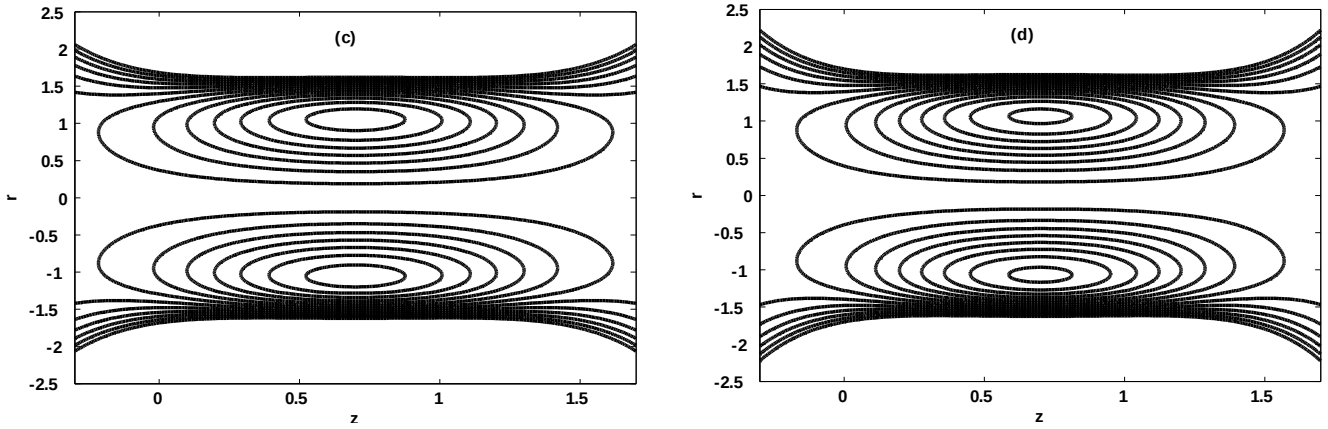

Figure 22. Stream lines for different values of n (c) $n = 2$ (d) $n = 4$ other parameters are $\phi = \pi,\ \varepsilon = 0.1,\ \delta = 0.01,\ \sigma_1 = 0.4,$ $We = 0.3,\ Q = 0.2.$

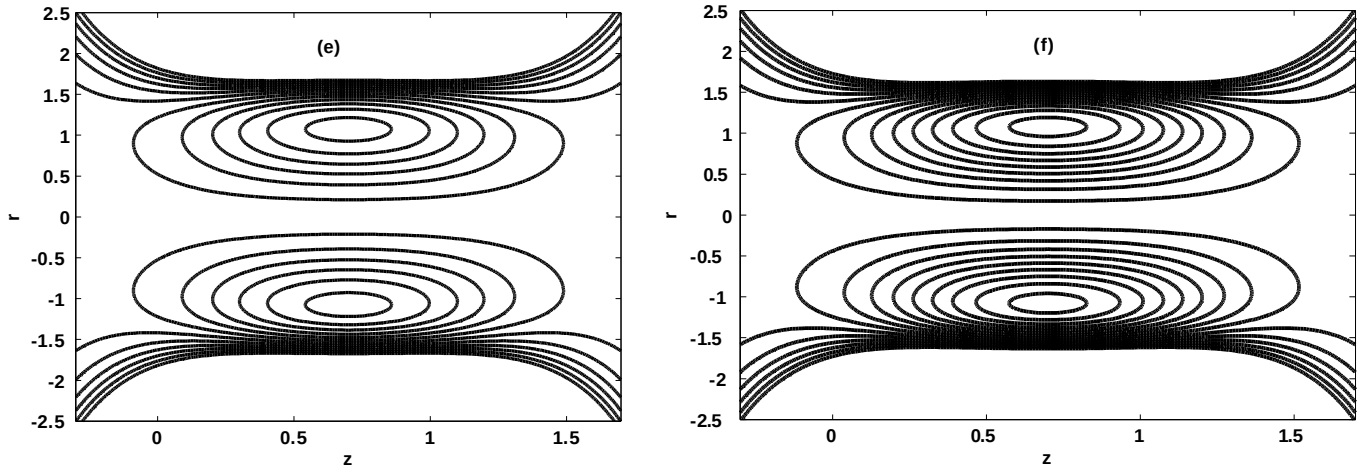

Figure 23. Stream lines for different values of We (e) $We = 0.1$ (f) $We = 0.2$ other parameters are $\phi = \pi,\ \varepsilon = 0.1,\ \delta = 0.1,\ \sigma = 0.4,$ $Q = 0.3,\ n = 2.$

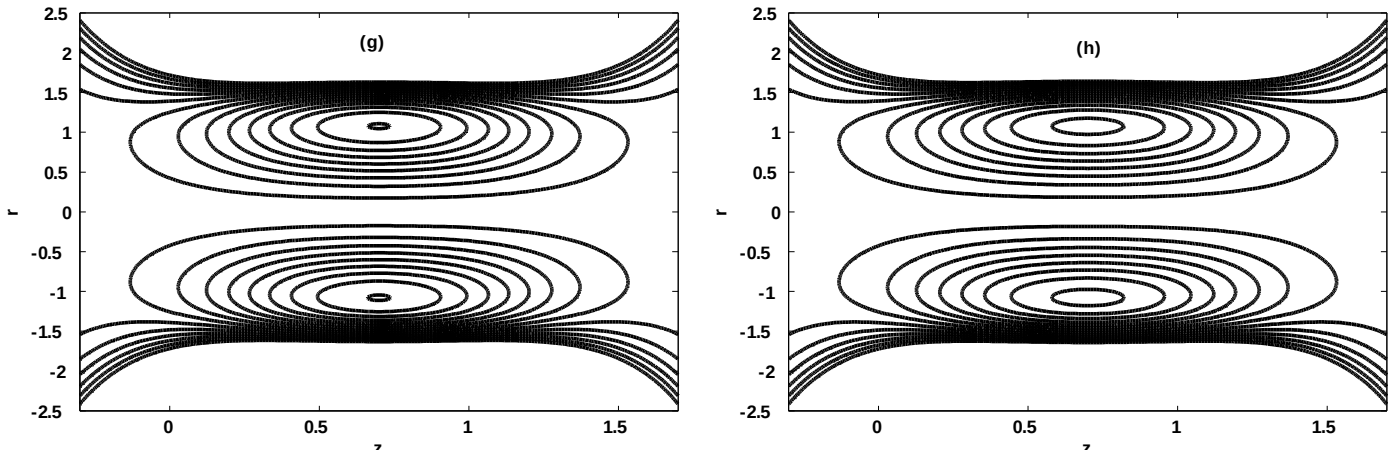

Figure 24. Stream lines for different values of ε (g) $\varepsilon = 0.1$ (h) $\varepsilon = 0.2$ other parameters are $\phi = \pi$, $We = 0.1$, $\delta = 0.1$, $\sigma = 0.4$, $Q = 0.3$, $n = 2$.

3) With an increase in We, δ and n shear stress decreases; the stress yield diverging tapering with tapered angle $\phi > 0$, converging tapering with tapered angle $\phi < 0$ and non-tapered artery with tapered angle $\phi = 0$.

4) We notice that the impedance resistance increases for converging tapering, diverging tapering and non-tapered arteries when we increase n and ε; while it decreases with increase in We.

5) It is analyzed through figures that shearing stress at the stenosis throat increases with an increase in ε, Q and We.

6) Temperature profile has opposite behaviour for Brickmann number B_r and Weissenberg number We.

7) It is analyzed that with an increase in Brickmann number B_r and Soret number S_r concentration profile decreases; while it increases with an increase in Weissenberg number We.

8) It is observed that with an increase in Weissenberg number We, the stenosis shape n and maximum height of the stenosis δ, number of trapping bolus increases and size of the trapping bolus decreases; while with an increase in extensional parameter ε, number of trapping bolus decreases and size of the trapping bolus increases.

REFERENCES

Abd El Hakeem AEN (2009). Creeping flow of Phan-Thien-Tanner fluids in a peristaltic tube with an infinite long wavelength. J. Appl. Mech. 76:1-6.

Afsar Khan A, Ellahi R, Vafai K (2012). Peristaltic transport of Jeffrey fluid with variable viscosity through a porous medium in an asymmetric channel. R. Adv. Anal. Meth. Math. Phys. 15:1-15.

Asghar S, Hayat T, Ellahi R (2008). Modelling of flow and heat transfer in a generalized second grade fluid. Int. J. Appl. Mech. Eng. 13(1):101-121.

Chakravarty S, Sen S (2005). Dynamic response of heat and mass transfer in blood flow through stenosed bifurcated arteries. Korea-Aust. Rheol. J. 17:47-62.

Ellahi R (2009). Effects of the slip boundary condition on non-Newtonian flows in a channel. Commun. Nonlin. Sci. Numer. Simul. 14(4):1377-1384.

Ellahi R (2010). Exact solutions of flows of an Oldroyd 8-constant fluid with nonlinear slip conditions. Z. Naturforsch. 65(a):1081-1086.

Ellahi R, Ariel PD, Hayat T, Asghar S (2010). Effect of heat transfer on a third grade fluid in a flat channel. Int. J. Numer. Meth. Fluids 63(7):847-859.

Kawase Y, Ulbrecht JJ (1983). Heat and mass transfer in non-Newtonian fluid flow with power function velocity profiles. Can. J. Chem. Eng. 61:791-800.

Khanafer K, Joseph L Bull, Pop I, Berguer R (2007). Influence of pulsatile blood flow and heating scheme on the temperature distribution during hyperthermia treatment. Int. J. Heat Mass Transf. 50:4883-4890.

Ma P, Li X, Ku DN (1994). Heat and mass transfer in a separated flow region for high Prandtl and Schmidt numbers under pulsatile conditions. Int. J. Heat Mass Transf. 37:2723-2736.

Mekheimer Kh S, El Kot MA (2008). The micropolar fluid model for blood flow through a tapered artery with a stenosis. Acta Mech. Sin. 24:637-644.

Nadeem S, Hayat, T, Noreen SA, Malik MY (2009). On the influence of heat transfer in peristalsis with variable viscosity. Int. J. Heat Mass Transf. 52:4722-4730.

Nadeem S, Noreen SA (2009). Influence of heat transfer on a peristaltic transport of Herschel--Bulkley fluid in a non-uniform inclined tube. Commun. Nonlin. Sci. Numer. Simul. 14:4100-4113.

Ogulu A, Abbey T M (2005). Simulation of heat transfer on an oscillatory blood flow in an indented porous artery. Int. Commun. Heat Mass Transf. 32:983-989.

Phan-Thien N (1978) A nonlinear network viscoelastic model. J. Rheol. 22:259-283.

Phan-Thien N, Tanner RI (1977). A new constitutive equation derived from network theory. J. Non-Newton. Fluid Mech. 2:353-365.

Valencia A, Villanueva M (2006). Unsteady flow and mass transfer in models of stenotic arteries considering fluid-structure interaction. Int. Commun. Heat Mass Transf. 33:966-975.